

1 **Turbidity hysteresis in an estuary and tidal river following an extreme discharge event**

2 David K. Ralston<sup>1</sup>, Brian Yellen<sup>2</sup>, Jonathan D. Woodruff<sup>2</sup>, Sarah Fernald<sup>3</sup>

3 <sup>1</sup> Woods Hole Oceanographic Institution, Woods Hole, MA, USA

4 <sup>2</sup> University of Massachusetts, Amherst, MA, USA

5 <sup>3</sup> New York State Department of Environmental Conservation, Hudson River National Estuarine Research  
6 Reserve, Staatsburg, NY, USA

7 [dralston@whoi.edu](mailto:dralston@whoi.edu), 508-289-2587

8 For *Geophysical Research Letters*

9 Submitted 16 Mar 2020, revised 27 Apr 2020

10 **Key points**

- 11 - Turbidity-discharge relationships are found in long-term observations ( $\geq 12$  years) at multiple  
12 locations along the tidal Hudson River  
13 - In the tidal freshwater, turbidity for a given discharge increased for 2 years following major  
14 discharge events and sediment input in 2011  
15 - In the saline estuary turbidity hysteresis was less apparent, consistent with greater background  
16 sediment concentrations and availability

17 **Abstract**

18 Non-linear turbidity-discharge relationships are explored in the context of sediment sourcing and event-  
19 driven hysteresis using long-term ( $\geq 12$  year) turbidity observations from the tidal freshwater and saline  
20 estuary of the Hudson River. At four locations spanning 175 km, turbidity generally increased with  
21 discharge but did not follow a constant log-log dependence, in part due to event-driven adjustments in  
22 sediment availability. Following major sediment inputs from extreme precipitation and discharge events  
23 in 2011, turbidity in the tidal river increased by 20-50% for a given discharge. The coherent shifts in the  
24 turbidity-discharge relationship along the tidal river over the subsequent 2 years suggest that the 2011  
25 events increased sediment availability for resuspension. In the saline estuary, changes in the sediment-  
26 discharge relationship were less apparent after the high discharge events, indicating that greater  
27 background turbidity due to internal sources make event-driven inputs less important in the saline estuary  
28 at interannual time scales.

29 **Plain language summary**

30 Turbidity is a widely accepted proxy for suspended sediment concentration and an important factor for  
31 contaminant transport and water quality. Here we show that turbidity depends on river discharge in long-  
32 term observations at multiple locations in an estuary. Such relationships are often used in rivers, but have  
33 not been commonly used in estuaries and tidal rivers, where tides and salinity also contribute to  
34 variability. Turbidity in the freshwater tidal region was more sensitive to discharge than in the saline  
35 estuary. Massive inputs of sediment due to extreme precipitation and flooding in 2011 resulted in  
36 increased sediment availability in the tidal river over multiple years. Turbidity throughout the tidal river  
37 was elevated for 2 years following the events, but changes were not apparent in the saline estuary. The  
38 observations provide guidance on recovery time scales for estuaries and tidal rivers to event-driven

39 sediment inputs, which affects the delivery of material from the watershed to the coastal ocean as well as  
40 other impacts relating to water clarity.

## 41 **1. Introduction**

42 Due to the challenges in continuously monitoring suspended sediment concentration (SSC), SSC and  
43 sediment discharge in rivers are often empirically related to volumetric freshwater discharge (Helsel and  
44 Hirsch 2002). Volumetric discharge varies by orders of magnitude at event and seasonal time scales, and  
45 it is the dominant factor controlling variability in sediment discharge. Sediment discharge increases  
46 nonlinearly with volumetric discharge, commonly increasing to approximately the cube of river discharge  
47 at high flow (Nash 1994; Syvitski et al. 2000). Consequently, large, relatively infrequent events  
48 disproportionately contribute to cumulative sediment discharges.

49 Sediment-discharge rating curves are often treated as static, and yet variability in precipitation patterns,  
50 vegetation, land use, and tectonic activity can all affect sediment delivery and sediment-discharge  
51 relationships (Walling 1977; Morehead et al. 2003; Warrick and Rubin 2007; Yellen et al. 2016).  
52 Disturbance from extreme floods can increase sediment concentrations for months to years as rivers  
53 adjust to bed incision and landslide scarps revegetate (Warrick et al. 2013; Dethier et al. 2016; Ahn et al.  
54 2017; Gray 2018). The duration and timing of low-discharge conditions can also affect in-stream storage  
55 and SSC during subsequent higher discharge periods (Walling et al. 1998; Gray et al. 2014). The  
56 sampling frequency can also contribute to uncertainty or introduce bias into measurement of sediment  
57 discharge (Coynel et al. 2004).

58 Rivers supply sediment to coastal regions, where tides, waves, and density-driven circulation also play  
59 central roles in sediment transport. In estuaries, salinity gradients drive landward near-bottom circulation  
60 that leads to sediment trapping and regions of higher sediment concentration, or estuarine turbidity  
61 maxima (ETMs) (Postma 1961; Burchard et al. 2018). River discharge alters sediment input from the  
62 watershed but also affects the salinity distribution, and thus the location and magnitude of sediment  
63 trapping at seasonal and event time scales. Tidal currents also contribute to variability in SSC, directly  
64 through sediment resuspension and indirectly by affecting the salinity distribution. In the tidal freshwater  
65 part of an estuary, tidal resuspension and sediment supply from the river are the key factors in SSC  
66 variability (Dalrymple and Choi 2007; Ralston and Geyer 2017). Tidal freshwater regions provide crucial  
67 links in the movement of material to the coastal ocean, and yet they have received less study than fluvial  
68 or estuarine environments (Hoitink and Jay 2016).

69 This study uses long-term ( $\geq 12$ -year) observations to characterize turbidity-discharge relationships in a  
70 tidal river and estuary, including the response following sediment inputs from major discharge events.  
71 Because it is easier to measure, turbidity is often used as a proxy for SSC (Yellen et al., 2014; Ahn et al.,  
72 2017), and turbidity has been shown to correlate well with SSC in the tidal river (Ralston and Geyer  
73 2017) and within the watershed (McHale and Siemion 2014). In late summer 2011, tropical cyclones  
74 Irene and Lee delivered intense precipitation over much of the U.S. Northeast, increasing discharge and  
75 sediment delivery. In the Delaware estuary, sediment input of 1.4 Mt in two weeks was similar to the  
76 long-term annual average, and SSC in the ETM remained elevated for several months (Sommerfield et al.  
77 2017). In the Connecticut River estuary, input from Irene of 1.2 Mt was twice the annual average, and the  
78 sediment-discharge relationship in the tidal river was elevated for the following 2 years compared to  
79 before the storm (Yellen et al. 2014). In the Hudson River estuary, sediment input from Irene and Lee was  
80 about 2.7 Mt, more than twice the annual average (Wall et al. 2008; Ralston et al. 2013). The events  
81 increased turbidity in the months following the events, but the response to this sediment input has not  
82 been examined at longer time scales. In this study we use long-term monitoring data to assess the

83 turbidity-discharge relationships at multiple locations along the tidal Hudson River and quantify the time  
84 scales over which the discharge events altered turbidity in the system.

## 85 **2. Methods**

### 86 *2.1 Site description*

87 The Hudson River estuary extends about 265 km from the Atlantic Ocean to tidal limit at Troy (NY).  
88 Along-estuary distances in the Hudson are typically reported with respect to The Battery in New York  
89 Harbor as 0 river km (rkm), but The Battery is located about 25 km landward of the natural mouth  
90 between Sandy Hook and Rockaway Peninsula. The tidal range averages about 1.5 m at the mouth,  
91 decreasing to 1 m mid-estuary and increasing to 1.5 m at the head of tides (Ralston et al. 2019). The  
92 salinity intrusion varies from about 40 rkm during high river discharge to 120 rkm during low discharge  
93 (Bowen and Geyer 2003; Ralston et al. 2008).

94 The primary ETM in the Hudson is located near 20 rkm, formed by bottom salinity fronts associated with  
95 a constriction (Geyer et al. 2001; Traykovski et al. 2004). During moderate and low discharge, a  
96 secondary ETM forms near 55 rkm (Nitsche et al. 2010; Ralston et al. 2012). In the primary ETM, near-  
97 bottom sediment concentrations can exceed  $1 \text{ g L}^{-1}$ , and concentrations are greater than  $100 \text{ mg/L}$  in much  
98 of the saline estuary. In the tidal river, sediment concentrations are generally less than  $100 \text{ mg L}^{-1}$  and  
99 vary with river discharge and tidal forcing (Wall et al. 2008; Ralston and Geyer 2017). Sediment inputs  
100 come from the two largest tributaries, the Mohawk and Upper Hudson Rivers, which converge just above  
101 the tidal limit. Numerous smaller tributaries also discharge into the tidal Hudson, cumulatively increasing  
102 the sediment load by 30-70% (Wall et al. 2008).

### 103 *2.2 Observations*

104 Turbidity data were collected from monitoring stations located along the estuary. Data were accessed  
105 through the Hudson River Environmental Conditions Observing System ([www.hrecos.org](http://www.hrecos.org)), which  
106 organizes monitoring data from multiple partner organizations, and the Centralized Data Management  
107 Office ([cdmo.baruch.sc.edu](http://cdmo.baruch.sc.edu)). Monitoring stations were at Schodack Island (212 rkm, available 2008-  
108 2019, partner organization Cary Institute of Ecosystem Studies), Tivoli North Bay (156 rkm, 2000-2019,  
109 Hudson River National Estuarine Research Reserve, HRNERR), Norrie Point (132 rkm, 2008-2019,  
110 HRNERR), and Piermont (37 rkm, 2008-2019, Lamont-Doherty Earth Observatory) (Fig. 1). Under most  
111 forcing conditions, Piermont is in the saline estuary and the other three stations are in the tidal freshwater  
112 (Hoitink and Jay 2016).

113 All stations recorded near-surface turbidity. Time series were processed for quality control based on  
114 visual inspection to remove spurious outliers or anomalous trends indicative of instrument fouling. The  
115 quality control removed 0.3% to 2.8% of the measurements, depending on the station. The Tivoli North  
116 Bay sensor is located in a small channel connecting to a side embayment, so we only used measurements  
117 during flood tides. Daily median turbidity values were used to minimize the influence of individual bad  
118 measurements on longer term variability. At Tivoli, water samples were collected, filtered, dried, and  
119 weighed to measure suspended solids concentration for comparison with turbidity. The regression slope  
120 for total suspended solids ( $\text{mg L}^{-1}$ ) was 1.2 times the turbidity (NTU,  $r^2 = 0.52$ ,  $n = 219$ ). Turbidity  
121 sensors at the other stations were not calibrated to SSC, but previous studies in the saline estuary and tidal  
122 river have also found calibrations with slopes of around 1 (Ralston et al. 2013; Ralston and Geyer 2017).

123 Volumetric discharge ( $Q_r$ ) and sediment discharge ( $Q_s$ ) measurements were collected from USGS gauging  
124 stations on the Mohawk and Upper Hudson. The Mohawk (at Cohoes, #01357500) has volumetric

125 discharge 1917-2019 and sediment discharge 1954-1959, 1976-1979, and 2002-2019. The Upper Hudson  
126 (Waterford, 01335770) has volumetric discharge 1887-1956 and 1976-2019, and sediment discharge  
127 1976-2014. Mean daily mean SSC were calculated with  $SSC = Q_s/Q_r$ .

128 Turbidity was related to  $Q_r$  by locally weighted scattered smoothing, or LOWESS (Cleveland 1979;  
129 Helsel and Hirsch 2002). The LOWESS approach has been used for sediment discharge rating curves in  
130 rivers, including in trend analyses following discharge events (Warrick et al. 2013; Gray 2018). LOWESS  
131 regressions were calculated for log-transformed discharge and turbidity with a smoothing factor of 0.25.  
132 A bias correction factor was included to calculate turbidity from discharge using the regression (Ferguson  
133 1986; Cohn 1995), with the form  $C = 10^{(C_{out} + \sigma^2/2)}$ , where  $C_{out}$  is the output from the LOWESS  
134 regression to  $\log_{10}(Q_r)$  and  $\sigma^2$  is the variance of the residual. The variance of the residual was calculated  
135 in fractional subsets of  $Q_r$  similar to the LOWESS smoothing factor to account for variability in the  
136 regression fit.

### 137 3. Results

138 Over the observation period (2008-2019), Irene and Lee accounted for the highest river discharge and  
139 observed turbidity (Fig. 1). The turbidity during and immediately following the 2011 events was greatest  
140 in the upper tidal river at Schodack Island, with 1000 NTU during Irene and 500 NTU during Lee. At the  
141 other stations in the tidal river, Tivoli North Bay and Norrie Point, turbidity was 200-300 NTU during the  
142 events. Increased turbidity was recorded during other high discharge periods, including spring freshets in  
143 2013, 2014, and 2016, but those maxima were less than half than during Irene. In the saline estuary, the  
144 Piermont station was not operational during the 2011 events. During other years, the maximum turbidity  
145 at Piermont was typically around 100 NTU, with generally higher turbidity during the winter and spring  
146 and lower in the summer.

147 Turbidity from the four stations is plotted against discharge, and all the locations have positive slopes  
148 (Fig. 2). At Schodack Island, the turbidity dependence on discharge has a form similar to many rivers  
149 (Nash 1994), with a greater slope at higher discharge ( $Q_r > 400 \text{ m}^3 \text{ s}^{-1}$ ), and weaker dependence at lower  
150  $Q_r$ . Schodack is in a shallow and sandy part of the tidal river (Nitsche et al. 2007; Collins and Miller  
151 2012), so resuspension of fine sediment is limited and turbidity varies strongly with river inputs. The  
152 slightly negative slope at low discharge may be an artifact of limited data, or may be due to increased  
153 organic particles during summer low discharge (Ralston and Geyer 2017). Farther seaward, at the Tivoli  
154 and Norrie Point stations, turbidity increases more gradually with discharge (Fig. 2b,c). Discharge varies  
155 annually by about an order of magnitude, and turbidity in the tidal river varies by more than an order of  
156 magnitude. The turbidity variability in the tidal freshwater river is greater than that in the saline estuary,  
157 where the annual range typically spans a factor of 2-3 (Bokuniewicz and Arnold 1984; Ralston et al.  
158 2012; Ralston and Geyer 2017). Correspondingly, the turbidity-discharge regression at Piermont has a  
159 narrower range than those at the upstream tidal river stations, and discharge dependence is weaker (Fig.  
160 2d). The LOWESS fits between discharge and turbidity at the tidal river stations had higher correlations  
161 ( $r^2 = 0.42$  at Schodack, 0.24 at Tivoli, and 0.19 at Norrie) than at Piermont in the saline estuary ( $r^2 =$   
162 0.12).

163 Scatter in the turbidity-discharge relationships is due to the many processes that affect turbidity in  
164 addition to discharge. Tidal amplitude affects sediment resuspension, and residuals in the LOWESS fits  
165 were positively correlated with tidal amplitude at all four locations, but the correlations were weak ( $r^2 <$   
166 0.005 at the tidal river stations and  $r^2 = 0.02$  at the estuarine Piermont station). Sediment resuspension and  
167 trapping can also vary with the salinity distribution, wind, and bed sediment properties. Lags in sediment  
168 transport can be weeks to months (Ralston and Geyer 2009; Ralston and Geyer 2017), distorting the

169 correspondence between the daily discharge and turbidity along the estuary. Antecedent discharge  
170 conditions affect sediment availability in the estuary, with fine sediment accumulating during higher  
171 discharge and subsequently increasing tidal resuspension, potentially changing the relationship with daily  
172 discharge (Wall et al. 2008).

173 To evaluate whether inputs from Irene and Lee affected sediment availability in the estuary and thus  
174 turbidity over longer time scales, the turbidity vs. discharge relationship is considered on a yearly basis.  
175 Turbidity time series are segmented by water year (October 1-September 30) to reflect the seasonality of  
176 higher discharge in the late fall, winter, and spring and lower discharge summer. As an example,  
177 observations for individual years are shown for Tivoli North Bay and compared to the regression for the  
178 entire record (Fig. 3). Clustering of median daily observations above or below the LOWESS fit of the full  
179 12-year record represents a shift in the turbidity-discharge relationship. Increased sediment availability  
180 following Irene and Lee corresponds to higher than average turbidity (for a given discharge) in 2012 and  
181 2013, as well as a few anomalously high turbidity observations during water year 2011 (Fig. 3d,e). In  
182 contrast, turbidity tends to be less than the long-term regression for most discharge conditions in 2015  
183 (Fig. 3g).

184 Over the turbidity observation period, the combined annual average discharge from Upper Hudson and  
185 Mohawk Rivers varied by almost a factor of 2, from  $350 \text{ m}^3 \text{ s}^{-1}$  to  $650 \text{ m}^3 \text{ s}^{-1}$ , and the maximum combined  
186 daily discharge varied by about a factor of 3, from  $1460 \text{ m}^3 \text{ s}^{-1}$  to  $4460 \text{ m}^3 \text{ s}^{-1}$  (Fig. 4a). Annual sediment  
187 inputs from the rivers were calculated based on observed discharge and regressions to long-term sediment  
188 discharge observations (Ralston et al. 2020), since the direct measurements of sediment discharge did not  
189 span the full period (Fig. 4b). The most notable variability in sediment inputs over this period was the  
190 large increase from the Mohawk with the storm events in 2011.

191 Annual averages of turbidity in the tidal freshwater and saline estuary varied by about a factor of 2 over  
192 the same period (Fig. 4c). The interannual variability in average turbidity is in part due to variation in  
193 river discharge, with higher turbidity during years with greater average discharge. However, the goal here  
194 is to assess whether hysteresis in the turbidity-discharge relationship may also contribute. To quantify  
195 this, we calculate the annual average of the ratio of the measured turbidity to that predicted by the  
196 turbidity-discharge regressions shown in Fig. 2. This turbidity ratio represents the factor by which the  
197 turbidity differed from the long-term regression, accounting for interannual variations in discharge (Fig.  
198 4d). Discretization at semi- and quarter-annual intervals was also examined, with similar (but noisier)  
199 results.

200 Similar interannual variation in turbidity relative to the long-term regression was observed among the  
201 three tidal freshwater stations (i.e. Schodack, Tivoli, and Norrie Point), despite separation of about 80 km  
202 and differences in local bed sediment. In 2012 and 2013, turbidity at all 3 locations was greater than  
203 expected based on the long-term regression, by factors of about 1.4 at Schodack, 1.3 at Tivoli, and 1.5 at  
204 Norrie. In 2010 and prior years, the turbidity factors were close to or less than 1 at all three stations. The  
205 turbidity factor increased at Tivoli and Norrie Point in 2011, but this could be due to large sediment  
206 inputs from tributaries near these stations during Irene and Lee at the end of 2011 water year (Ralston et  
207 al. 2013). After 2013, the turbidity ratios returned to values similar to 1, representing a return to long-term  
208 average conditions, with values less than 1 before and after 2011-2014 potentially explained by the long-  
209 term regression including the elevated turbidity from Irene and Lee. Average turbidity in the tidal river  
210 thus depended both on  $Q_r$  that year and on hysteresis in the turbidity-discharge relationship. For example,  
211 the mean  $Q_r$  in 2012 ( $390 \text{ m}^3 \text{ s}^{-1}$ ) was less than average ( $460 \text{ m}^3 \text{ s}^{-1}$ ), and yet the average turbidity that year  
212 was the second highest overall (Fig. 4c). In 2013 the turbidity increased in part because the discharge  
213 increased, but also because of the above-average turbidity-discharge relationship (Fig. 4d).

214 Another approach to characterizing the temporal variability in the turbidity-discharge relationship is to  
215 calculate the slope of the cumulative residual between the observed and predicted turbidity (Gray 2018).  
216 Periods when observed turbidity was greater than expected have a positive slope for the cumulative  
217 residual, and periods with turbidity less than expected have a negative slope. Results using the cumulative  
218 residual slopes were consistent with the turbidity ratios, with positive slopes during years with turbidity  
219 ratio greater than 1 and negative residuals for turbidity ratios less than 1 (Suppl. Fig. 1). Similarly, the  
220 cumulative residual slopes at the tidal river stations were maximum in 2012 and 2013, after Irene and  
221 Lee, and decreased to zero or negative values in 2014 or 2015.

222 The temporal variability in the turbidity-discharge relationship was coherent among the freshwater tidal  
223 stations, but observations in the saline estuary did not exhibit the same interannual response (Fig. 4c). For  
224 example, the turbidity ratio at Tivoli was strongly correlated with that at Norrie Point ( $r^2 = 0.93$ ,  $p < 0.001$ ,  
225  $n=11$ ) and had a weaker correlation with Schodack Island ( $r^2 = 0.63$ ,  $p=0.028$ ,  $n=12$ ), but the correlation  
226 with Piermont in the saline estuary was not significant ( $r^2 = 0.33$ ,  $p=0.35$ ,  $n=10$ ). The Piermont station  
227 exhibited only a modest increase in the turbidity ratio in 2012 after Irene and Lee (with a data gap in  
228 2013), and in general has less variability in the turbidity-discharge relationship.

229 The turbidity ratios in the estuary were not significantly correlated with the year-to-year variability in the  
230 sediment mass inputs from the Mohawk and Upper Hudson (Fig. 4b). To evaluate the influence of the  
231 variability in watershed inputs, we also calculated the residual of the LOWESS regressions of  $\log_{10}(SSC)$   
232 vs.  $\log_{10}(Q_r)$  for the tributaries on an annual basis. Precipitation from Irene and Lee was focused in the  
233 Mohawk watershed and the Catskill Mountains east of the Hudson, leading to mass wasting, increased  
234 erosion, and potential hysteresis in the sediment-discharge relationship for these regions (Ahn and  
235 Steinschneider 2019). In water years 2012-2014 following the events, the average SSC in the Mohawk  
236 increased by a factor of about 1.2 above the regression values, but the Mohawk turbidity ratio was not  
237 significantly correlated with the turbidity ratios in the estuary. As expected from precipitation patterns  
238 during Irene-Lee, the turbidity-discharge ratio for the Upper Hudson did not change post-event.

#### 239 **4. Summary and discussion**

240 Long-term monitoring data allow for characterization of turbidity-discharge relationships in the estuary  
241 that might be obscured by variability at tidal to seasonal time scales. In the tidal freshwater, turbidity  
242 depended strongly on discharge (Fig. 2). Average residuals between observed turbidity and that predicted  
243 from the discharge regressions were coherent among stations in the tidal river, with increased turbidity in  
244 the 2 years following tropical storms Irene and Lee (Fig. 4). Similarly, in New England watersheds  
245 adjustment time scales for channel morphology following Irene, and for subsequent, smaller discharge  
246 events, were found to be 1-2 years (Renshaw et al. 2019). Watershed sediment supply also depends on  
247 revegetation of landslides and bank failures, which adjusts at multi-year time scales (Gray et al. 2014;  
248 Yellen et al. 2014; Dethier et al. 2016). In the tidal Hudson, variations in the turbidity residuals in the  
249 estuary were not directly tied to the interannual sediment inputs from the two largest tributaries, which  
250 suggests that increased sediment availability for resuspension in the tidal river led to hysteresis in the  
251 sediment-discharge relationship. The similar response among stations separated by 80 km suggests that  
252 the increased sediment availability was not limited to a small region or due to localized influence of a  
253 particular tributary.

254 Increased turbidity suggests an increase in SSC, particularly for a fixed particle size distribution.  
255 Alternatively, temporal decreases in the dominant particle size could increase turbidity and change the  
256 relationship to SSC (Downing 2006). Seasonal variation in the slope between turbidity and SSC of about  
257 a factor of 2 has been noted in the tidal Hudson, likely due to changes in particle size with discharge

258 (Ralston and Geyer 2017). Thus the shift toward higher turbidity ratios may reflect a combination of  
259 greater availability and finer grain size following discharge events (Yellen et al. 2016). The contribution  
260 of organic material to turbidity also varies seasonally, as on average SPM samples in summer and fall had  
261 higher organic fractions than in the first half of the year. However, our averaging of turbidity ratios at  
262 annual time scales reduces effects of seasonal variation in the relationship between turbidity and SPM on  
263 discharge dependence. Due to the relatively turbid conditions and low light availability, phytoplankton  
264 are also not expected to contribute significantly to the turbidity signal (Cole et al. 1992).

265 The turbidity responses differed between the tidal river and saline estuary, where changes in the turbidity-  
266 discharge relationship were less apparent following the discharge events. In the tidal river, SSC tends to  
267 be lower and the bed less muddy than in the saline estuary (Nitsche et al. 2007). The sediment available  
268 for resuspension at event to seasonal time scales has been termed the mobile sediment pool (Wellershaus  
269 1981; Schoellhamer 2011; Geyer and Ralston 2018). While the size of the mobile pool is difficult to  
270 quantify, the persistent increase in turbidity in the tidal river following Irene and Lee suggests that the  
271 sediment input from the storms represented a major increase in the size of the mobile pool. Based on  
272 sediment flux time series, about 2/3 of the sediment input by the events remained in the tidal river several  
273 months after the events (Ralston et al. 2013), and the 2-year period of increased turbidity may be  
274 indicative of the time scale for the tidal river to adjust back to pre-storm conditions.

275 In the saline estuary, turbidity on average is greater, the bed is muddier, and the mobile pool is larger than  
276 in the tidal river. Previous studies have highlighted the seasonal to annual variation in SSC and deposition  
277 (Geyer et al. 2001; Woodruff et al. 2001). Observations in the lower ETM found that the freshets in 1998  
278 and 1999 each deposited about 0.3 Mt of new sediment, despite large differences in the watershed  
279 sediment inputs in those years (Woodruff et al. 2001). This decoupling between deposition in the ETM  
280 and the watershed inputs is consistent with the limited variability in the turbidity-discharge residual at  
281 Piermont. If the mobile pool in the saline estuary is many times the annual average input, then the  
282 fractional increase from Irene and Lee may be minor. Similarly, in San Francisco Bay a decrease in  
283 sediment supply associated with dam construction did not affect sediment concentrations until decades  
284 later, first in the tidal freshwater Delta and subsequently in the saline estuary (Schoellhamer 2011; Hestir  
285 et al. 2013; Schoellhamer et al. 2013). In the Penobscot estuary, the mobile sediment pool was estimated  
286 to be 6-8 times the annual average input based on recovery time scales following a contaminant release  
287 (Geyer and Ralston 2018).

288 Differences between the tidal river and saline estuary in the hysteresis of the turbidity-discharge  
289 relationships reflect the relative coupling between sediment supply and river discharge. In the saline  
290 estuary, the mobile pool is large compared to the annual supply, such that a major discharge event does  
291 not drastically increase sediment availability. In contrast, fine grained bed sediment in the tidal river is  
292 more limited, so event inputs represent a fractionally bigger change, and turbidity is increased for a  
293 couple of years as the added sediment gradually moves seaward and deposits in lower energy shoals and  
294 wetlands (Ralston and Geyer 2017; Yellen et al. 2020). For comparison, the hysteresis in turbidity-  
295 discharge relationship in the tidal river is similar in duration to observations on steep streams following  
296 Irene (Renshaw et al., 2019), but shorter in duration than observed in rivers along the U.S. West Coast,  
297 where sediment concentrations remained elevated for 5 years or longer after events (Warrick et al. 2013;  
298 Gray 2018). Long-term measurements at stream gauging stations allow for assessment of the variability in  
299 turbidity/sediment-discharge relationships in the watershed, but such long-term measurements are far less  
300 common in estuaries. These results point to the utility of such measurements for assessing the multiple  
301 time scales of sediment variability in other estuaries.

## 302 **Acknowledgements**

303 This work was sponsored by the National Estuarine Research Reserve System Science Collaborative,  
304 funded by the National Oceanic and Atmospheric Administration and managed by the University of  
305 Michigan Water Center (NAI4NOS4190145), with additional support to Yellen and Woodruff from  
306 USGS Cooperative Agreement No. G19AC00091. The data used in this study were all downloaded from  
307 publicly available sources (USGS, HRECOS, or CDMO) as described in the Methods section.

## 308 **References**

- 309 Ahn, Kuk-Hyun, and Scott Steinschneider. 2019. Time-varying, nonlinear suspended sediment rating  
310 curves to characterize trends in water quality: An application to the Upper Hudson and Mohawk  
311 Rivers, New York. *Hydrological Processes* 33: 1865–1882. doi:10.1002/hyp.13443.
- 312 Ahn, Kuk-Hyun, Brian Yellen, and Scott Steinschneider. 2017. Dynamic linear models to explore time-  
313 varying suspended sediment-discharge rating curves. *Water Resources Research* 53: 4802–4820.
- 314 Bokuniewicz, Henry J., and Chester L. Arnold. 1984. Characteristics of suspended sediment transport in  
315 the lower Hudson River. *Northeastern Environmental Science* 3: 184–189.
- 316 Bowen, Melissa M., and W. Rockwell Geyer. 2003. Salt transport and the time-dependent salt balance of  
317 a partially stratified estuary. *Journal of Geophysical Research* 108: 3158.  
318 doi:10.1029/2001JC001231.
- 319 Burchard, Hans, Henk M. Schuttelaars, and David K. Ralston. 2018. Sediment Trapping in Estuaries.  
320 *Annual Review of Marine Science* 10: null. doi:10.1146/annurev-marine-010816-060535.
- 321 Cleveland, William S. 1979. Robust locally weighted regression and smoothing scatterplots. *Journal of*  
322 *the American statistical association* 74: 829–836.
- 323 Cohn, T. A. 1995. Recent advances in statistical methods for the estimation of sediment and nutrient  
324 transport in rivers. *Reviews of Geophysics* 33: 1117–1123. doi:10.1029/95RG00292.
- 325 Cole, Jonathan J., Nina F. Caraco, and Benjamin L. Peierls. 1992. Can phytoplankton maintain a positive  
326 carbon balance in a turbid, freshwater, tidal estuary? *Limnology and Oceanography* 37: 1608–  
327 1617. doi:10.4319/lo.1992.37.8.1608.
- 328 Collins, M. J., and D. Miller. 2012. Upper Hudson River Estuary (usa) Floodplain Change Over the 20th  
329 Century. *River Research and Applications* 28: 1246–1253. doi:10.1002/rra.1509.
- 330 Coynel, Alexandra, Jörg Schäfer, Jean-Emmanuel Hurtrez, Jacques Dumas, Henri Etcheber, and Gérard  
331 Blanc. 2004. Sampling frequency and accuracy of SPM flux estimates in two contrasted drainage  
332 basins. *Science of The Total Environment* 330: 233–247. doi:10.1016/j.scitotenv.2004.04.003.
- 333 Dalrymple, Robert W., and Kyungsik Choi. 2007. Morphologic and facies trends through the fluvial–  
334 marine transition in tide-dominated depositional systems: a schematic framework for  
335 environmental and sequence-stratigraphic interpretation. *Earth-Science Reviews* 81: 135–174.
- 336 Dethier, Evan, Francis J. Magilligan, Carl E. Renshaw, and Keith H. Nislow. 2016. The role of chronic  
337 and episodic disturbances on channel–hillslope coupling: the persistence and legacy of extreme  
338 floods. *Earth Surface Processes and Landforms* 41: 1437–1447.
- 339 Downing, John. 2006. Twenty-five years with OBS sensors: The good, the bad, and the ugly. *Continental*  
340 *Shelf Research* 26. Special Issue in Honor of Richard W. Sternberg’s Contributions to Marine  
341 Sedimentology: 2299–2318. doi:10.1016/j.csr.2006.07.018.
- 342 Ferguson, R. I. 1986. River loads underestimated by rating curves. *Water resources research* 22: 74–76.
- 343 Geyer, W. Rockwell, and D. K. Ralston. 2018. A mobile pool of contaminated sediment in the Penobscot  
344 Estuary, Maine, USA. *Science of The Total Environment* 612: 694–707.  
345 doi:10.1016/j.scitotenv.2017.07.195.
- 346 Geyer, W. Rockwell, Jonathan D. Woodruff, and Peter Traykovski. 2001. Sediment Transport and  
347 Trapping in the Hudson River Estuary. *Estuaries* 24: 670–679.
- 348 Gray, A. B., J. A. Warrick, G. B. Pasternack, E. B. Watson, and M. A. Goñi. 2014. Suspended sediment  
349 behavior in a coastal dry-summer subtropical catchment: Effects of hydrologic preconditions.  
350 *Geomorphology* 214: 485–501. doi:10.1016/j.geomorph.2014.03.009.

351 Gray, Andrew B. 2018. The impact of persistent dynamics on suspended sediment load estimation.  
352 *Geomorphology* 322: 132–147.

353 Helsen, Dennis R., and Robert M. Hirsch. 2002. *Statistical methods in water resources*. Vol. 323. US  
354 Geological Survey Reston, VA.

355 Hestir, Erin L., David H. Schoellhamer, Tara Morgan-King, and Susan L. Ustin. 2013. A step decrease in  
356 sediment concentration in a highly modified tidal river delta following the 1983 El Niño floods.  
357 *Marine Geology* 345. A Multi-Discipline Approach for Understanding Sediment Transport and  
358 Geomorphic Evolution in an Estuarine-Coastal System: San Francisco Bay: 304–313.  
359 doi:10.1016/j.margeo.2013.05.008.

360 Hoitink, A. J. F., and D. A. Jay. 2016. Tidal river dynamics: Implications for deltas. *Reviews of*  
361 *Geophysics* 54: 2015RG000507. doi:10.1002/2015RG000507.

362 Lumia, Richard, Gary D. Firda, and Travis L. Smith. 2014. *Floods of 2011 in New York*. US Department  
363 of the Interior, US Geological Survey.

364 McHale, Michael R., and Jason Siemion. 2014. *Turbidity and suspended sediment in the upper Esopus*  
365 *Creek watershed, Ulster County, New York*. Scientific Investigations Report 2014–5200. U.S.  
366 Geological Survey.

367 Morehead, Mark D., James P. Syvitski, Eric WH Hutton, and Scott D. Peckham. 2003. Modeling the  
368 temporal variability in the flux of sediment from ungauged river basins. *Global and Planetary*  
369 *change* 39: 95–110.

370 Nash, D. B. 1994. Effective sediment-transporting discharge from magnitude-frequency analysis. *Journal*  
371 *of Geology* 102: 79–96.

372 Nitsche, F.O., T.C. Kenna, and M. Haberman. 2010. Quantifying 20th century deposition in complex  
373 estuarine environment: An example from the Hudson River. *Estuarine, Coastal and Shelf Science*  
374 89: 163–174. doi:10.1016/j.ecss.2010.06.011.

375 Nitsche, F.O., W.B.F. Ryan, S.M. Carbotte, R.E. Bell, A. Slagle, C. Bertinado, R. Flood, T. Kenna, and  
376 C. McHugh. 2007. Regional patterns and local variations of sediment distribution in the Hudson  
377 River Estuary. *Estuarine, Coastal and Shelf Science* 71: 259–277.  
378 doi:10.1016/j.ecss.2006.07.021.

379 Postma, H. 1961. Transport and accumulation of suspended matter in the Dutch Wadden Sea.  
380 *Netherlands Journal of Sea Research* 1: 148–180.

381 Ralston, David K., and W. Rockwell Geyer. 2009. Episodic and Long-Term Sediment Transport Capacity  
382 in The Hudson River Estuary. *Estuaries and Coasts* 32: 1130–1151. doi:10.1007/s12237-009-  
383 9206-4.

384 Ralston, David K., and W. Rockwell Geyer. 2017. Sediment transport time scales and trapping efficiency  
385 in a tidal river. *Journal of Geophysical Research: Earth Surface* 122: 2042–2063.

386 Ralston, David K., W. Rockwell Geyer, and James A. Lerczak. 2008. Subtidal Salinity and Velocity in  
387 the Hudson River Estuary: Observations and Modeling. *Journal of Physical Oceanography* 38:  
388 753–770.

389 Ralston, David K., W. Rockwell Geyer, and John C. Warner. 2012. Bathymetric controls on sediment  
390 transport in the Hudson River estuary: Lateral asymmetry and frontal trapping. *Journal of*  
391 *Geophysical Research* 117: C10013. doi:10.1029/2012JC008124.

392 Ralston, David K., Stefan Talke, W. Rockwell Geyer, Hussein A. M. Al-Zubaidi, and Christopher K.  
393 Sommerfield. 2019. Bigger Tides, Less Flooding: Effects of Dredging on Barotropic Dynamics in  
394 a Highly Modified Estuary. *Journal of Geophysical Research: Oceans* 124: 196–211.  
395 doi:10.1029/2018JC014313.

396 Ralston, David K., John C. Warner, W. Rockwell Geyer, and Gary R. Wall. 2013. Sediment transport due  
397 to extreme events: The Hudson River estuary after tropical storms Irene and Lee. *Geophysical*  
398 *Research Letters* 40: 2013GL057906. doi:10.1002/2013GL057906.

399 Ralston, David K., Brian Yellen, and Jonathan D. Woodruff. 2020. Watershed sediment supply and  
400 potential impacts of dam removals for an estuary. Submitted manuscript. DOI:  
401 10.1002/essoar.10502519.1. ESSOAr.

402 Renshaw, Carl E., Francis J. Magilligan, Helen G. Doyle, Evan N. Dethier, and Keith M. Kantack. 2019.  
403 Rapid response of New England (USA) rivers to shifting boundary conditions: Processes, time  
404 frames, and pathways to post-flood channel equilibrium. *Geology* 47. GeoScienceWorld: 997–  
405 1000. doi:10.1130/G46702.1.

406 Schoellhamer, David H. 2011. Sudden Clearing of Estuarine Waters upon Crossing the Threshold from  
407 Transport to Supply Regulation of Sediment Transport as an Erodible Sediment Pool is Depleted:  
408 San Francisco Bay, 1999. *Estuaries and Coasts* 34: 885–899. doi:10.1007/s12237-011-9382-x.

409 Schoellhamer, David H., Scott A. Wright, and Judith Z. Drexler. 2013. Adjustment of the San Francisco  
410 estuary and watershed to decreasing sediment supply in the 20th century. *Marine Geology* 345:  
411 63–71.

412 Sommerfield, Christopher K., Daniel I. Duval, and Robert J. Chant. 2017. Estuarine sedimentary response  
413 to Atlantic tropical cyclones. *Marine Geology* 391: 65–75. doi:10.1016/j.margeo.2017.07.015.

414 Syvitski, James P., Mark D. Morehead, David B. Bahr, and Thierry Mulder. 2000. Estimating fluvial  
415 sediment transport: The rating parameters. *Water Resources Research* 36: 2747–2760.  
416 doi:10.1029/2000WR900133.

417 Traykovski, Peter, W. Rockwell Geyer, and Chris Sommerfield. 2004. Rapid sediment deposition and  
418 fine-scale strata formation in the Hudson estuary. *Journal of Geophysical Research* 109: F02004.  
419 doi:10.1029/2003JF000096.

420 Wall, G., E. Nystrom, and S. Litten. 2008. Suspended Sediment Transport in the Freshwater Reach of the  
421 Hudson River Estuary in Eastern New York. *Estuaries and Coasts*. doi:10.1007/s12237-008-  
422 9050-y.

423 Walling, D. E. 1977. Assessing the accuracy of suspended sediment rating curves for a small basin. *Water*  
424 *Resources Research* 13: 531–538.

425 Walling, Desmond E., Philip N. Owens, and Graham J. L. Leeks. 1998. The role of channel and  
426 floodplain storage in the suspended sediment budget of the River Ouse, Yorkshire, UK.  
427 *Geomorphology* 22: 225–242. doi:10.1016/S0169-555X(97)00086-X.

428 Warrick, J. A., Mary Ann Madej, M. A. Goñi, and R. A. Wheatcroft. 2013. Trends in the suspended-  
429 sediment yields of coastal rivers of northern California, 1955–2010. *Journal of hydrology* 489:  
430 108–123.

431 Warrick, Jonathan A., and David M. Rubin. 2007. Suspended-sediment rating curve response to  
432 urbanization and wildfire, Santa Ana River, California. *Journal of Geophysical Research: Earth*  
433 *Surface* 112.

434 Wellershaus, St. 1981. Turbidity maximum and mud shoaling in the Weser estuary. *Archiv für*  
435 *Hydrobiologie* 92.

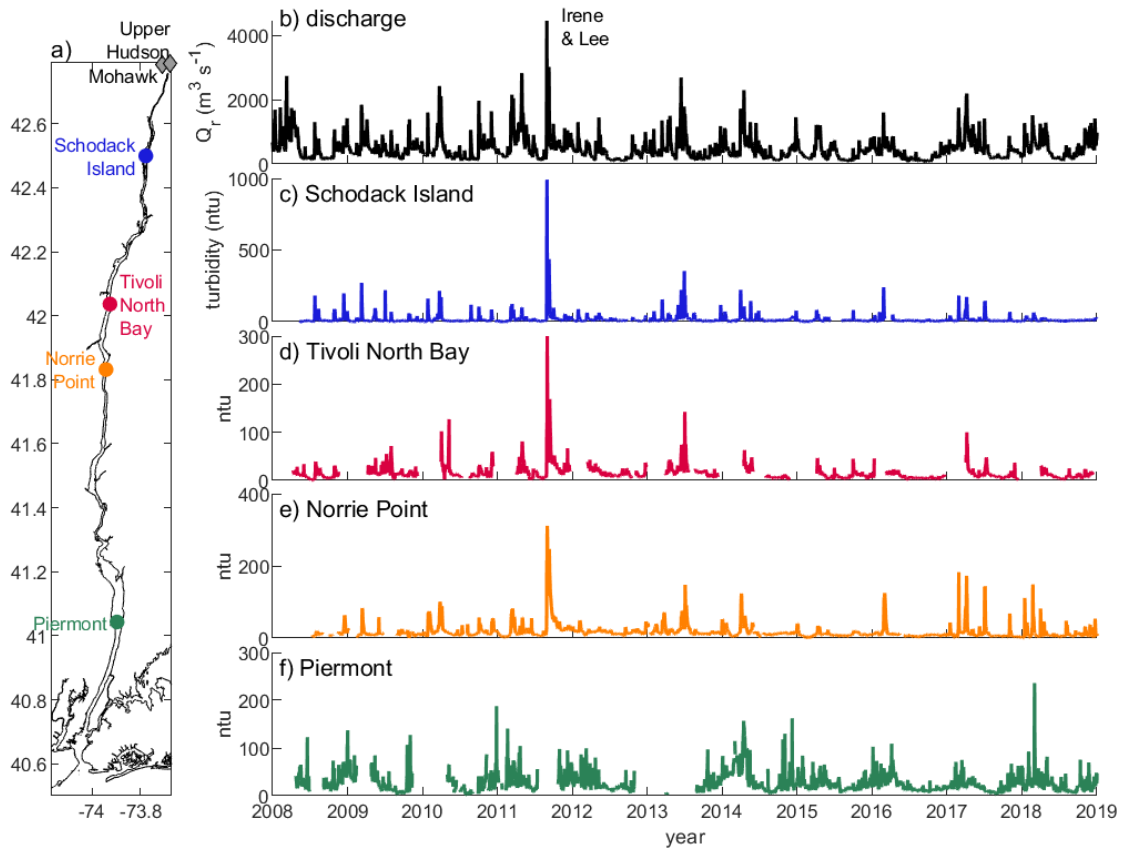
436 Woodruff, Jonathan D., W. Rockwell Geyer, Christopher K. Sommerfield, and Neal W. Driscoll. 2001.  
437 Seasonal variation of sediment deposition in the Hudson River estuary. *Marine Geology* 179:  
438 105–119. doi:10.1016/S0025-3227(01)00182-7.

439 Yellen, B., J. D. Woodruff, L. N. Kratz, S. B. Mabee, J. Morrison, and A. M. Martini. 2014. Source,  
440 conveyance and fate of suspended sediments following Hurricane Irene. New England, USA.  
441 *Geomorphology* 226: 124–134.

442 Yellen, Brian, Jonathan D. Woodruff, Timothy L. Cook, and Robert M. Newton. 2016. Historically  
443 unprecedented erosion from Tropical Storm Irene due to high antecedent precipitation. *Earth*  
444 *Surface Processes and Landforms* 41: 677–684. doi:10.1002/esp.3896.

445 Yellen, Brian, Jonathan D. Woodruff, Caroline Ladlow, David K. Ralston, Sarah Fernald, and Waverly  
446 Lau. 2020. Rapid Tidal Marsh Development in Anthropogenic Backwaters. EarthArXiv.  
447

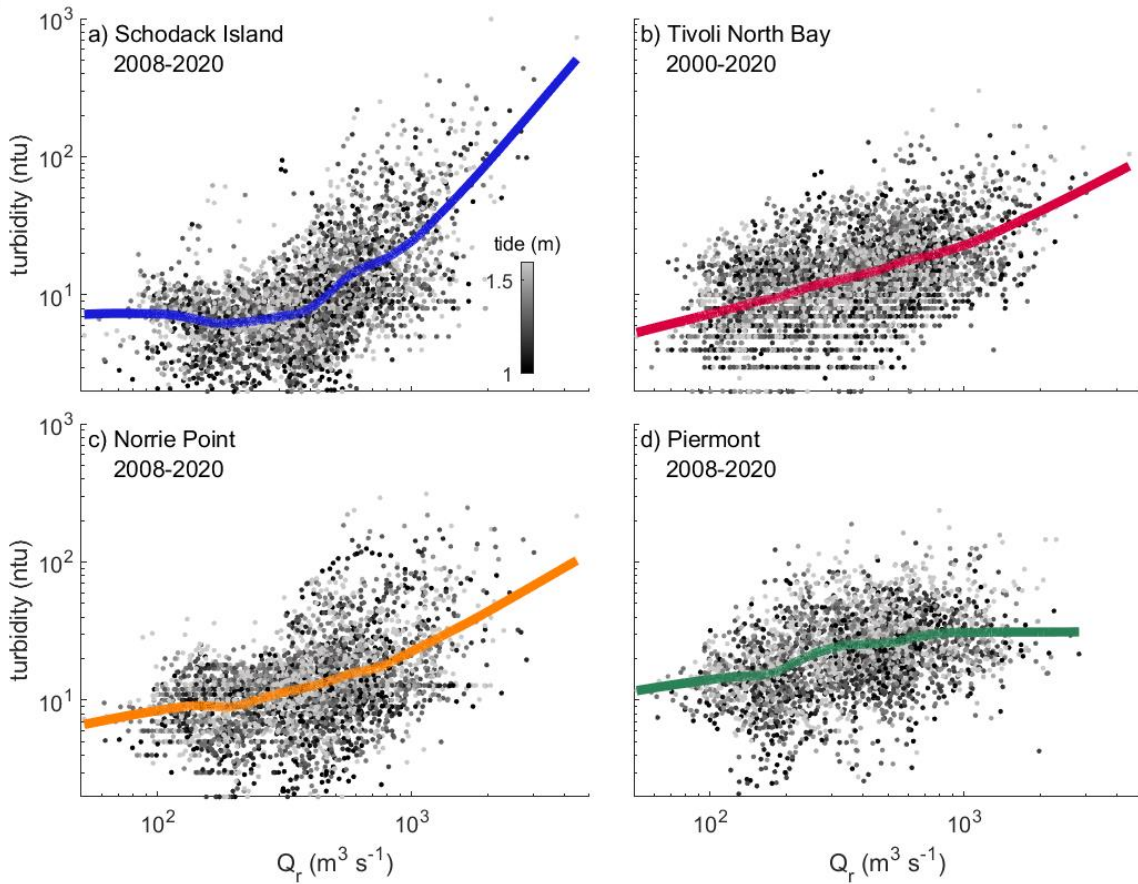
Figure 1



449

450 **Figure 1.** Turbidity at monitoring stations along the estuary. a) Station locations, b) daily average  
 451 discharge from the Upper Hudson and Mohawk, noting Tropical Storms Irene and Lee in 2011, c-f) daily  
 452 median turbidity from Schodack Island, Tivoli North Bay, Norrie Point, and Piermont.

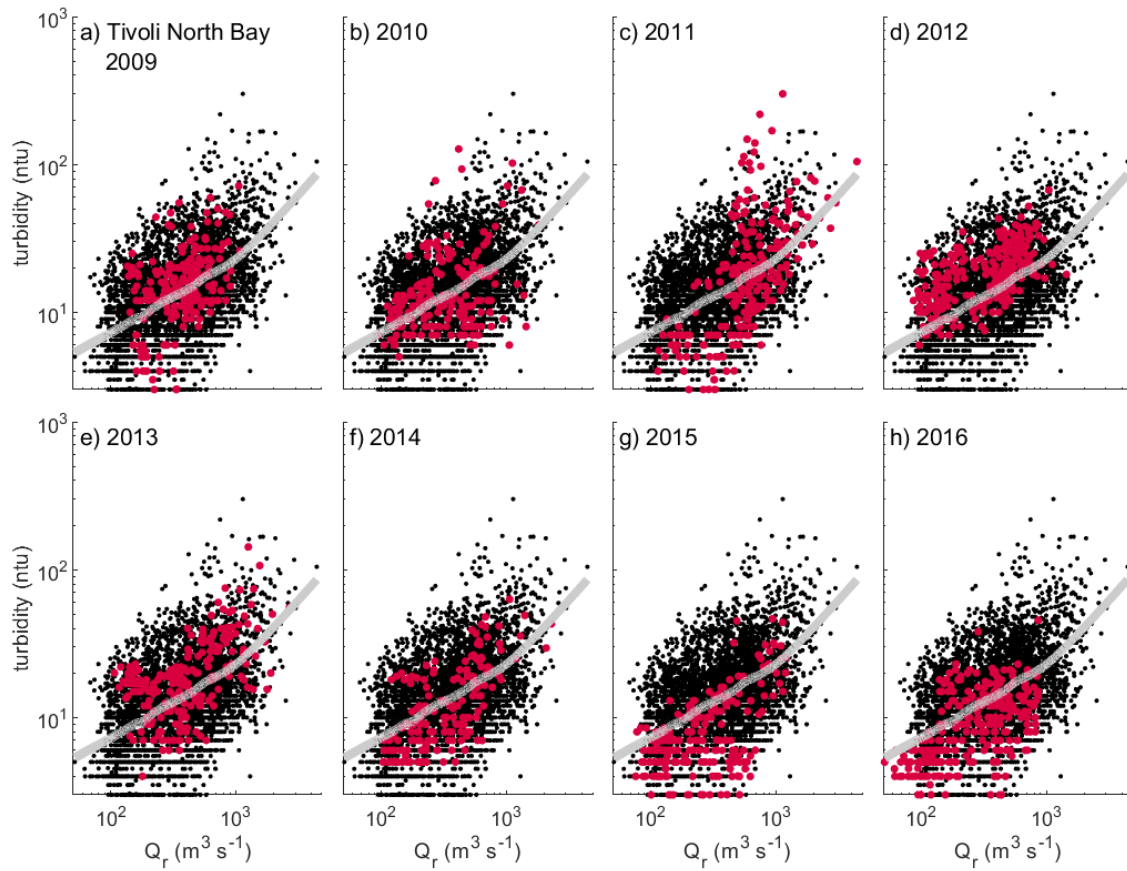
Figure 2



453

454 **Figure 2.** Turbidity vs. river discharge a) at Schodack Island, b) Tivoli North Bay, c) Norrie Point, and d)  
455 Piermont. Daily turbidity data are in black and LOWESS regressions are colored. Marker shading  
456 represents tidal amplitude based on the tidal water level range at The Battery (NOAA # 8518750), located  
457 near the mouth of the Hudson.

Figure 3



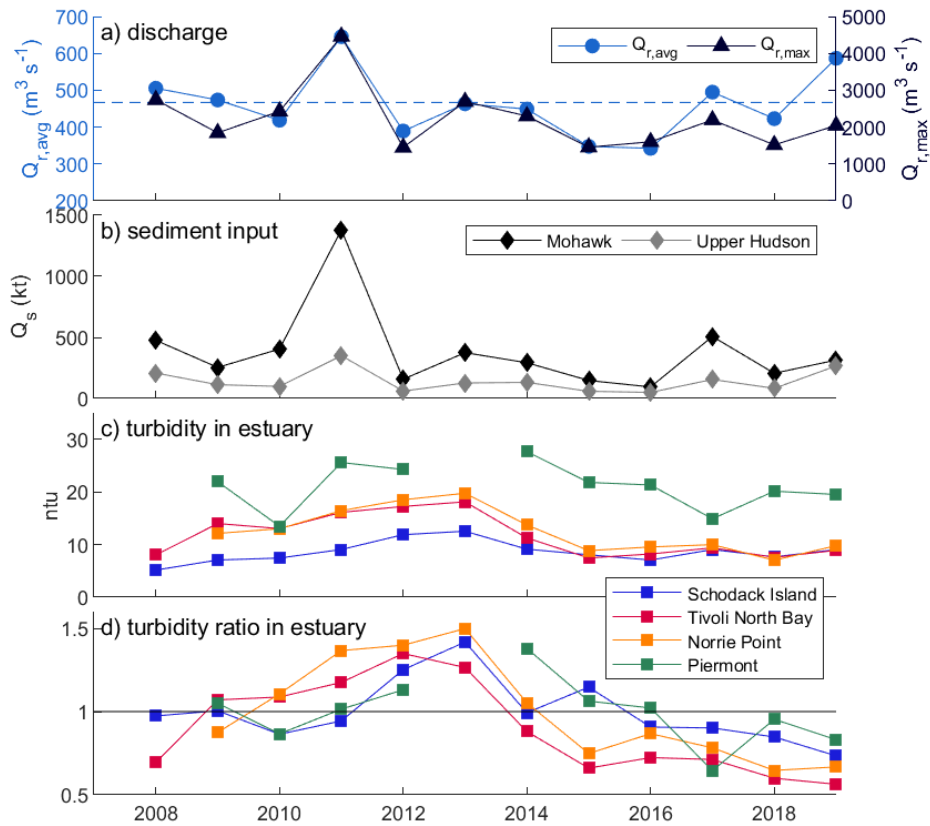
458

459 **Figure 3.** Turbidity vs. river discharge at Tivoli North Bay by water year from 2009 to 2016. The full  
460 record is in black, and data for each year are colored. The LOWESS fit to the full record is gray.

461

462

Figure 4

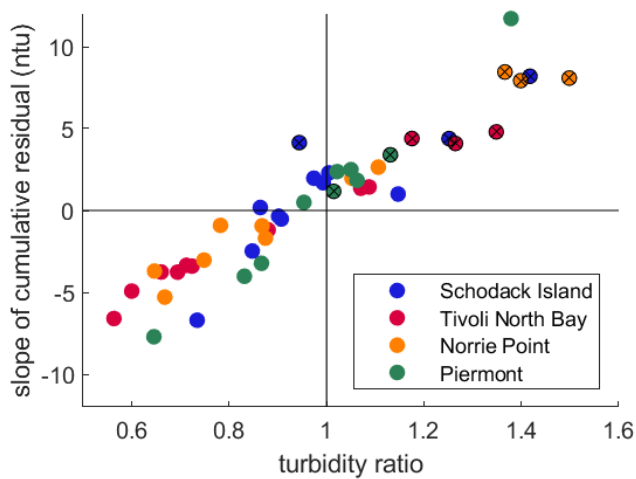


463

464 **Figure 4.** Discharge and turbidity by water year. a) Mean and maximum discharge of the Upper Hudson  
 465 and Mohawk rivers, b) annual sediment input from the Mohawk and Upper Hudson, c) annual average  
 466 turbidity in the tidal river and estuary, d) annual average of the ratio of measured turbidity to that  
 467 predicted by the long-term  $Q_r$  regressions (Fig. 2).

468

S1



469

470 **Figure S1.** Annual averages of the slope of the cumulative residual vs. turbidity ratio. Turbidity ratio  
471 same as in Fig. 4d. Positive slopes and turbidity ratios greater than 1 correspond with years when the  
472 turbidity vs. discharge relationship was greater than the long-term regression. The years following  
473 Tropical Storms Irene and Lee (2011-2013) are marked with an 'x'.

Figure 1.

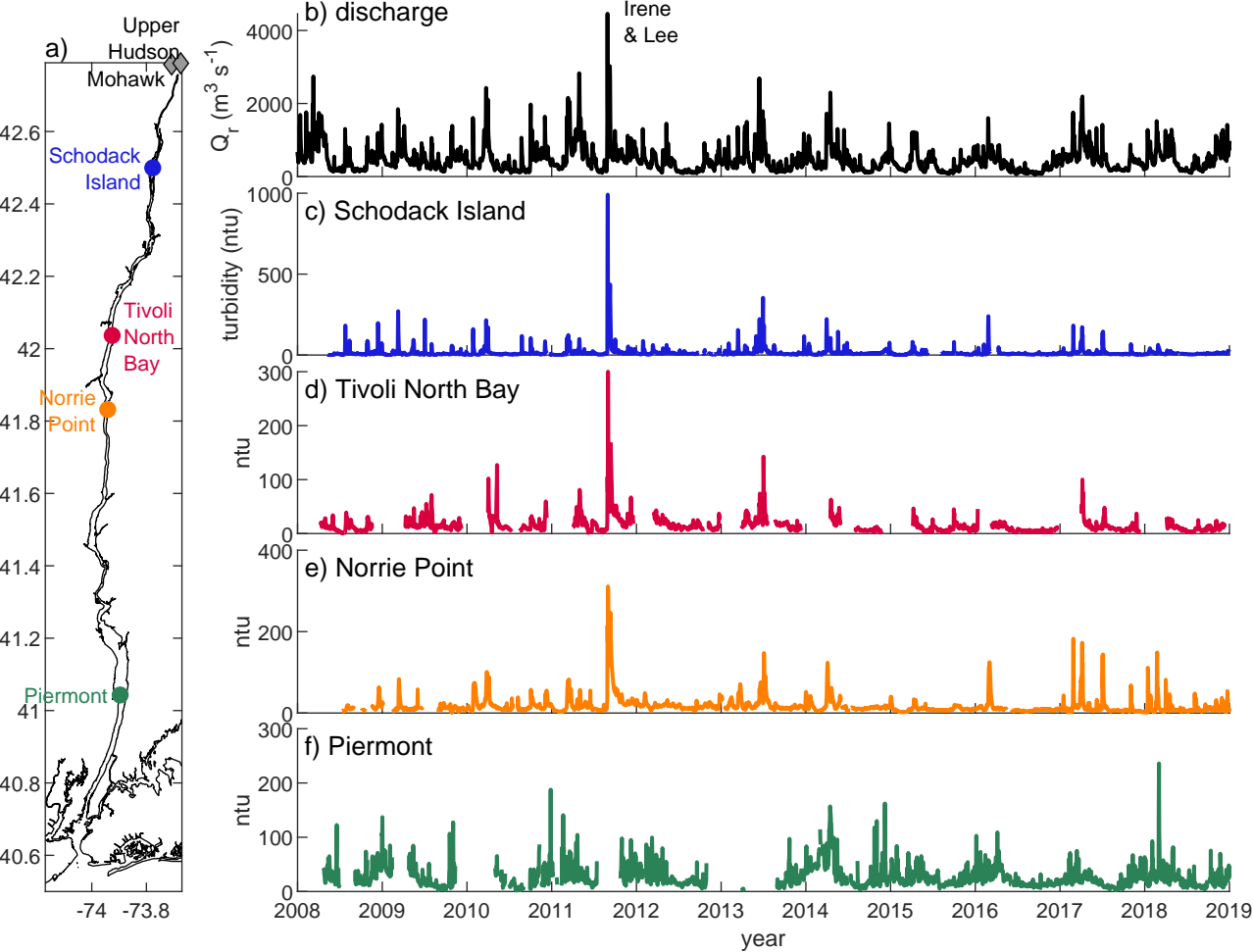


Figure 2.

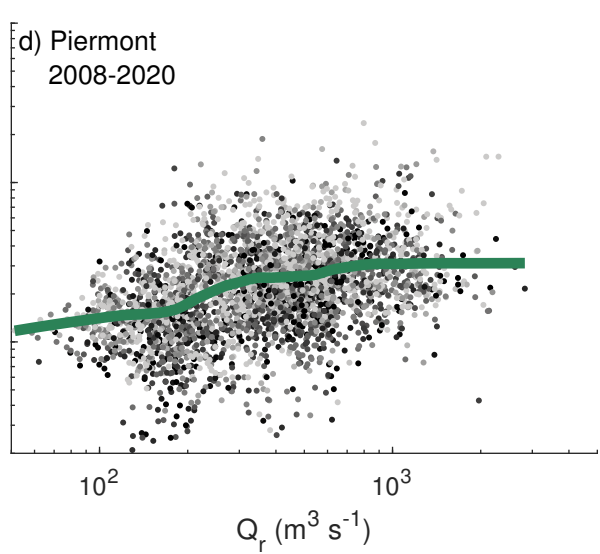
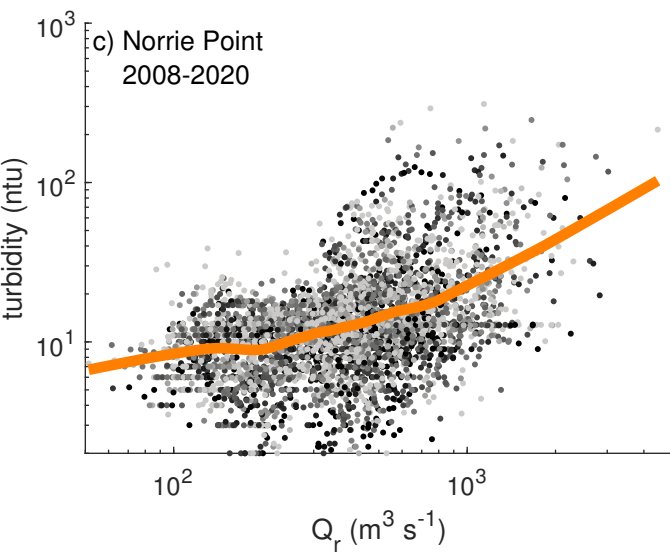
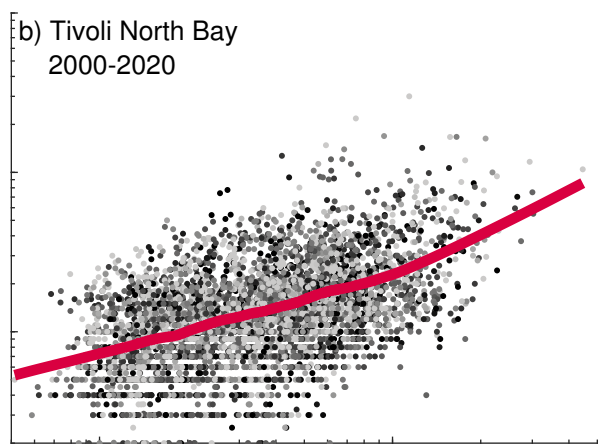
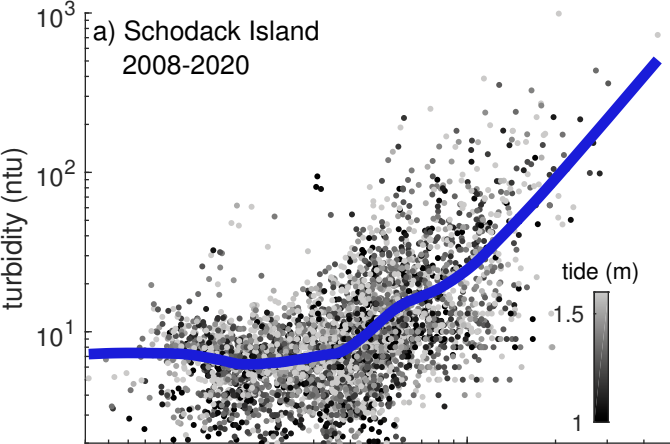
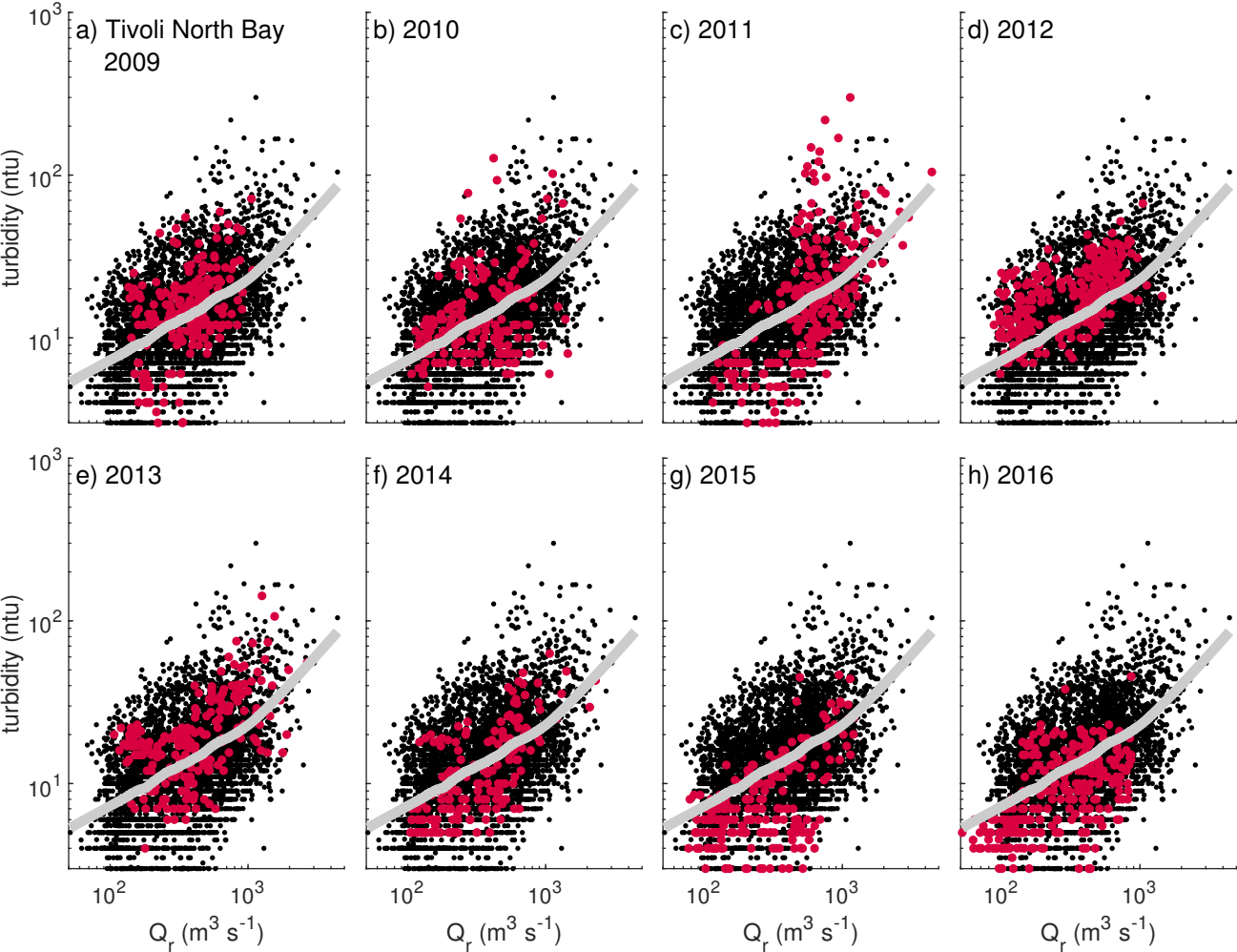


Figure 3.



**Figure 4.**

